

Towards a universal QAOA protocol: Evidence of quantum advantage in solving combinatorial optimization problems

J. A. Montañez-Barrera^{1,*} and Kristel Michiels^{1,2,3}

¹*Jülich Supercomputing Centre, Institute for Advanced Simulation,
Forschungszentrum Jülich, 52425 Jülich, Germany*

²*AIDAS, 52425 Jülich, Germany*

³*RWTH Aachen University, 52056 Aachen, Germany*

The quantum approximate optimization algorithm (QAOA) is a promising algorithm for solving combinatorial optimization problems (COPs). In this algorithm, there are alternating layers consisting of a mixer and a problem Hamiltonian. Each layer $i = 0, \dots, p - 1$ is parameterized by β_i and γ_i . How to find these parameters has been an open question with the majority of the research focused on finding them using classical algorithms. In this work, we present evidence that fixed linear ramp schedules constitute a universal set of QAOA parameters, i.e., a set of γ and β parameters that rapidly approximate the optimal solution, x^* , independently of the COP selected, and that the success probability to find it, $\text{probability}(x^*)$, increases with the number of QAOA layers p . We simulate linear ramp QAOA protocols (LR-QAOA) involving up to $N_q = 42$ qubits and $p = 400$ layers on random instances of 9 different COPs. The results suggest that $\text{probability}(x^*) \approx 1/2^{(\eta N_q/p)}$ for a constant η . We extend the analysis in 4 COPs with $p = N_q$ and show that $\text{probability}(x^*)$ seems to be constant for general cases. For example, when implementing LR-QAOA with $p = 42$, the $\text{probability}(x^*)$ for 42-qubit Weighted MaxCut problems (W-MaxCut) increases from $2/2^{42} \approx 10^{-13}$ to an average of 0.13. We compare LR-QAOA, simulated annealing (SA), and branch-and-bound (B&B) finding a fundamental improvement in LR-QAOA. We test LR-QAOA on real hardware using IonQ Aria, Quantinuum H2-1, IBM Brisbane, IBM Kyoto, and IBM Osaka, encoding random weighted MaxCut (W-MaxCut) problems from 5 to 109 qubits and $p = 3$ to 100. We find that even for the largest case, $N_q = 109$ qubits and $p = 100$, information about the LR-QAOA optimization protocol is still present. The circuit involved requires 21200 CNOT gates and a time of $\approx 132 \mu\text{s}$. The resilience of LR-QAOA to noise is attributed to its characteristic of bringing the system towards a minimal energy state despite noise driving it towards a maximally mixed state. These results show that LR-QAOA is effective in finding high-quality solutions for COPs and suggest an advantage of quantum computation for combinatorial optimization in the near future.

Keywords: Combinatorial Optimization, QAOA, LR-QAOA, traveling salesman, maximal independent set, bin packing, portfolio optimization, weighted maxcut, knapsack, MAX-3-SAT, .

I. INTRODUCTION

Finding high-quality solutions for COPs is perceived as one of the main applications of quantum computation in the near future. In the gate-based regime, QAOA [1] has become one of the most studied quantum algorithms for solving COPs. There are different factors for the extensive study of QAOA. Firstly, parametric unitary gates can effectively represent the Hamiltonian of the COPs, where the ground state encodes the optimal solution of the problem [2, 3]. Moreover, QAOA has a performance guarantee in the limit of infinite layers resembling the quantum adiabatic algorithm [1, 4]. Additionally, QAOA needs fewer resources (e.g. number of gates and qubits) compared to other quantum algorithms and can be tested on current state-of-the-art quantum hardware [5–7]. Furthermore, classical methods find it hard to solve large instances of COPs with practical applications [8], and therefore finding alternative ways to solve them is needed.

Ultimately, the goal of quantum optimization algorithms, as exemplified by QAOA, is to demonstrate advantages in solving optimization problems, be it in terms of energy efficiency, time-to-solution (TTS), or solution quality compared to classical methods.

In the simplest version of QAOA, the cost Hamiltonian of a combinatorial optimization problem is encoded in a parametric unitary gate along with a “mixer”, a second parametric unitary gate that does not commute with the first unitary gate. In this context, parameters $\gamma = [\gamma_0, \dots, \gamma_{p-1}]$ and $\beta = [\beta_0, \dots, \beta_{p-1}]$ for the cost and mixer Hamiltonians, respectively, are adjusted to minimize the expectation value of the cost Hamiltonian for $i = 0, \dots, p - 1$ layers of QAOA. Since its conception, a classical algorithm was suggested to find the QAOA γ and β parameters [1]. This makes QAOA fall in the category of variational quantum algorithms (VQA) [9]. However, these algorithms have exhibited a limited/poor performance advantage as the classical optimization part finds it hard to escape local minima when searching for γ and β parameters [10, 11].

Modest progress has been made by thinking of QAOA as a VQA, with major studies conducted in regimes of a few qubits and shallow circuits [5]. Deep QAOA cir-

* Corresponding author: J. A. Montañez-Barrera; j.montanez-barrera@fz-juelich.de

culits, when viewed through the lens of VQA, lead to a pessimistic conclusion regarding their universal applicability [12]. Moreover, implementations on real hardware face an even greater challenge, the noise inherent in current quantum devices makes the search for the minima of the objective function unfeasible after only a few QAOA layers [12, 13].

Alternatively to this methodology, one can fix the γ and β parameters following some protocol, similar to what quantum annealing (QA) does [14, 15]. In this scenario, no further classical optimization is needed.

Initial evidence supporting the effectiveness of fixed-parameter QAOA was presented by Brandao et al. [16]. They demonstrated that fixed parameters exhibit consistent performance regardless of the problem or problem size, suggesting the potential reduction of the outer loop of classical optimization in QAOA.

Various protocols have been proposed to fix these parameters. In [11], Kremenetski et. al. found a set of QAOA parameters with consistent performance to find optimal solutions using a fixed LR-QAOA protocol. They tested this methodology using the Hamiltonian of different molecules, an Ising Hamiltonian, and the 3-SAT problem for intermediate to large p . Another attempt for fixing the QAOA protocol is proposed in [17], in which the authors presented QAOA as a second-order time discretization of QA referred to as approximate quantum annealing (AQA). LR-QAOA can be considered as an AQA protocol with a linear annealing schedule.

In [18], we proposed fixed schedules transferring optimal γ and β parameters between different COPs. We found that γ and β parameters that work well for a COP eventually give good results in other COPs independently of the COP structure. This information led us to the results of the present work.

Recently, Kremenetski et. al. have explained the behavior of LR-QAOA and in general of the gradually changing schedules using the discrete adiabatic theorem involving a wrap-around phenomenon [19].

In this paper, we extend the study of LR-QAOA schedules to different COPs presenting analytical, numerical, and experimental evidence that LR-QAOA constitutes a universal QAOA protocol, i.e., the set of γ and β parameters from a linear ramp schedule that work effectively independently of the problem or problem size in combinatorial optimization. We test this protocol using maximal independent set (MIS), bin packing (BPP), traveling salesman (TSP), maximum cut (MaxCut), weighted maximum cut (W-MaxCut), 3-regular graph maximum cut (3-MaxCut), Knapsack (KP), portfolio optimization (PO), 2 Boolean satisfiability problem (Max-2-SAT), and maximum 3-SAT (Max-3-SAT). We use random instances of these COPs with problem sizes ranging from 4 to 42 qubits and p from 3 to 400. For large problems, we simulate them using JUQCS-G software [17] on JUWELS Booster, a cluster of 3744 NVIDIA A100 Tensor Core GPUs, integrated into the modular supercomputer JUWELS [20, 21].

In these cases, the average probability of success over the 5 random instances seems to follow a scaling that can be described by $probability(x^*) = 1/2^{(\eta N_q/p)}$ for a constant η . We extend the analysis on 4 different problems keeping the relation $p = N_q$, expecting $probability(x^*)$ to stay constant. We use fully connected random W-MaxCut, MaxCut, Max-2-SAT, and Max-3-SAT. The W-MaxCut, MaxCut, and Max-3-SAT are both NP-Hard [22] and APX-Hard [23] problems, and we show that the time-to-solution (TTS) [13] using our selected instances of W-MaxCut indeed grows exponentially when using classical optimizers.

We find a fundamental improvement in terms of the TTS when using LR-QAOA with the probability of success on average remaining constant $probability(x^*) = 1/2^\eta$ using $p = N_q$. With this further evidence, we conjecture that the expected probability of success will follow the relation $probability(x^*) = 1/2^{(\eta N_q/p)}$ for general cases of COPs. If this conjecture holds, it implies that there is a quantum algorithm that in polynomial time can solve instances of NP-Hard problems that are already hard for classical algorithms. However, we note that for some cases, the relation $probability(x^*) = 1/2^{(\eta N_q/p)}$ seems not to hold. We attributed it to the high concentration of sub-optimal solution close to the optimal. Even if the conjecture does not hold, there is a noticeable scaling advantage in LR-QAOA compared to these classical solvers.

We extend the analysis to real quantum hardware. Using IonQ Aria (*ionq-aria*), Quantinuum H2-1 (*quantinuum-H2*) [24], IBM Brisbane (*ibm-brisbane*), IBM Kyoto (*ibm-kyoto*), and IBM Osaka (*ibm-osaka*), we run W-MaxCut problems ranging from 5 to 109 qubits and p from 3 to 100. We find that there is an effective number of layers, p_{eff} , for which the best performance is obtained using each device. In the case of IBM devices $p_{\text{eff}} = 10$, on *ionq-aria* $p_{\text{eff}} = 10$, and on *quantinuum-H2* $p_{\text{eff}} = 50$. Remarkably, for the largest problem size, 109 qubits and $p = 100$, we observe some information about the LR-QAOA optimization is still preserved in *ibm-kyoto* and *ibm-osaka*. For a comparative analysis between the different vendors, we test a 25-qubit W-MaxCut problem on them, *quantinuum-H2* gives the best performance with a $probability(x^*) = 0.08$ at $p = 50$.

We demonstrate that LR-QAOA is resilient against noise. This robustness is attributed to the interplay of two opposing forces. While noise pushes the system towards a maximally mixed state, LR-QAOA drives the system towards the minimum energy of the cost Hamiltonian correcting errors on the way. To explore this phenomenon, we conduct simulations using a Qiskit Aer noise model [25] on a 10-qubit W-MaxCut problem. We vary the strengths of depolarizing noise affecting the 2-qubit gates within the algorithm. Our findings show significant alignment with the behavior exhibited by *ionq-aria* when solving the same problem.

The rest of the paper is organized as follows. Section II provides a description of the LR-QAOA protocol,

its universal properties, a description of the COPs used, the classical solvers used for comparison, the Hamiltonian normalization, the performance diagram, the mitigation technique, the experimental details, and the noise simulation. In Sec. III, we present our results and a discussion for simulation and experimentation using the given protocol. Finally, Sec. IV contains our conclusions.

II. METHODS

A. LR-QAOA

QAOA consists of alternating layers that encode the problem of interest along with a mixer element in charge of amplifying the desired solutions with low energy. In this case, the COP cost Hamiltonian is given by

$$H_C = \sum_i h_i \sigma_z^i + \sum_{i,j>i} J_{ij} \sigma_z^i \sigma_z^j, \quad (1)$$

where σ_z^i is the Pauli-z term of qubit i , and h_i and J_{ij} are coefficients associated with the problem. Usually, H_C is derived from the quadratic unconstrained binary optimization (QUBO) formulation [2, 18, 26]. The QUBO to H_C transformation usually includes a constant term that does not affect the QAOA formulation and is left out for simplicity. H_C is encoded into a parametric unitary gate given by

$$U_C(H_C, \gamma) = e^{-j\gamma_i H_C}, \quad (2)$$

where γ_i is a parameter that in our case comes from the linear ramp schedule. Following this, in every second layer, a unitary operator is applied given by

$$U(H_B, \beta) = e^{j\beta_i H_B}, \quad (3)$$

where β_i is taken from the linear ramp schedule and $H_B = \sum_{i=0}^{N_q-1} \sigma_i^x$ with σ_i^x the Pauli-x term of qubit i . The general QAOA circuit is shown in Fig. 1-(a). Here, $R_X(-2\beta_i) = e^{j\beta_i \sigma^x}$, p is the number of repetitions of the unitary gates of Eqs. 2 and 3, and the initial state is a superposition state $|+\rangle^{\otimes N_q}$. Repeated preparation and measurement of the final QAOA state yields a set of candidate solution samples, which are expected to give the optimal solution or some low-energy solution.

In Fig. 1-(b), we show the LR-QAOA protocol. It is characterized by three parameters Δ_β , Δ_γ , and the number of layers p . The β_i and γ_i parameters are given by

$$\beta_i = \left(1 - \frac{i}{p}\right) \Delta_\beta \quad \text{and} \quad \gamma_i = \frac{i+1}{p} \Delta_\gamma, \quad (4)$$

for $i = 0, \dots, p-1$. For our simulations and experimental results, we use $\Delta_\beta = 0.3$ and $\Delta_\gamma = 0.6$. In the extended simulations for the conjecture, we use $\Delta_\beta = \Delta_\gamma = \Delta_{\gamma,\beta} = 0.5$ and $\Delta_{\gamma,\beta} = 0.4$. The special property of a linear ramp schedule is the constant slope Δ_γ/p .

B. Universal properties of LR-QAOA

The QAOA evolution is usually presented from the point of view of the expectation value of the cost Hamiltonian [1, 19, 27]. In this section, we present a framework where the evolution under LR-QAOA is seen from the point of view of the individual amplitudes of all possible states in a COP. The state vector that describes the evolution of $\text{probability}(x^*)$ of a COP is given by

$$|\psi_t\rangle = \sum_{k=0}^{2^{N_q}-1} \alpha_k^t |k\rangle, \quad (5)$$

where t is some step in the QAOA algorithm, k are the states in the computational basis, and α_k^t the amplitude of $|k\rangle$ at time t .

The unitary transformation induced by $U_C(\gamma_t)$ produces a rotation in the complex plane for every state given by

$$\alpha_k^{t+1} = e^{i\theta_k^t} \alpha_k^t, \quad (6)$$

$$\theta_k^t = E_k \gamma_t, \quad (7)$$

where $E_k = \langle k | H_C | k \rangle$, and $|k\rangle$ is the state k , e.g., $|0010\rangle$. This evolution is shown in Fig. 2 (a). Equation 7 explains why the amplitude amplification is proportional to the energy of a given solution. Negative energies are rotated counterclockwise with the rotation proportional to their energies. This can be seen in Fig. 2-(e).

The change by $U_B(\beta_t)$ is more complex and depends on the Hamming distance of the given state to the other states. This operator is responsible for the change in energy and produces an interference pattern that exploits the $U_C(\gamma_t)$ effect. It is described by

$$\alpha_k^{t+1} = \sum_{l=0}^{2^q-1} (\cos(\beta_t))^{N_q-k \cdot l} (j \sin(\beta_t))^{k \cdot l} \alpha_l^t, \quad (8)$$

with

$$k \cdot l = \sum_{m=0}^{N_q-1} (k_2[m] + l_2[m]) \mod 2, \quad (9)$$

where k_2 (l_2) is the binary representation of k (l). Equation 9 gives the Hamming distance between the state k and l . For example, in a 3-qubit system, the evolution of α_{000}^t is given by

$$\begin{aligned} \alpha_{000}^{t+1} &= \langle 000 | U_B(\beta_t) | \psi_t \rangle \\ &= \cos^3(\beta_t) \alpha_{000}^t \\ &\quad + j \sin(\beta_t) \cos^2(\beta_t) (\alpha_{001}^t + \alpha_{010}^t + \alpha_{100}^t) \\ &\quad - \sin^2(\beta_t) \cos(\beta_t) (\alpha_{011}^t + \alpha_{101}^t + \alpha_{110}^t) \\ &\quad - j \sin^3(\beta_t) \alpha_{111}^t. \end{aligned}$$

A schematic representation of how the $U_B(\beta_t)$ induces an evolution of α_{000} is shown in Fig. 2-(b). Here, $U_B(\beta_t)$

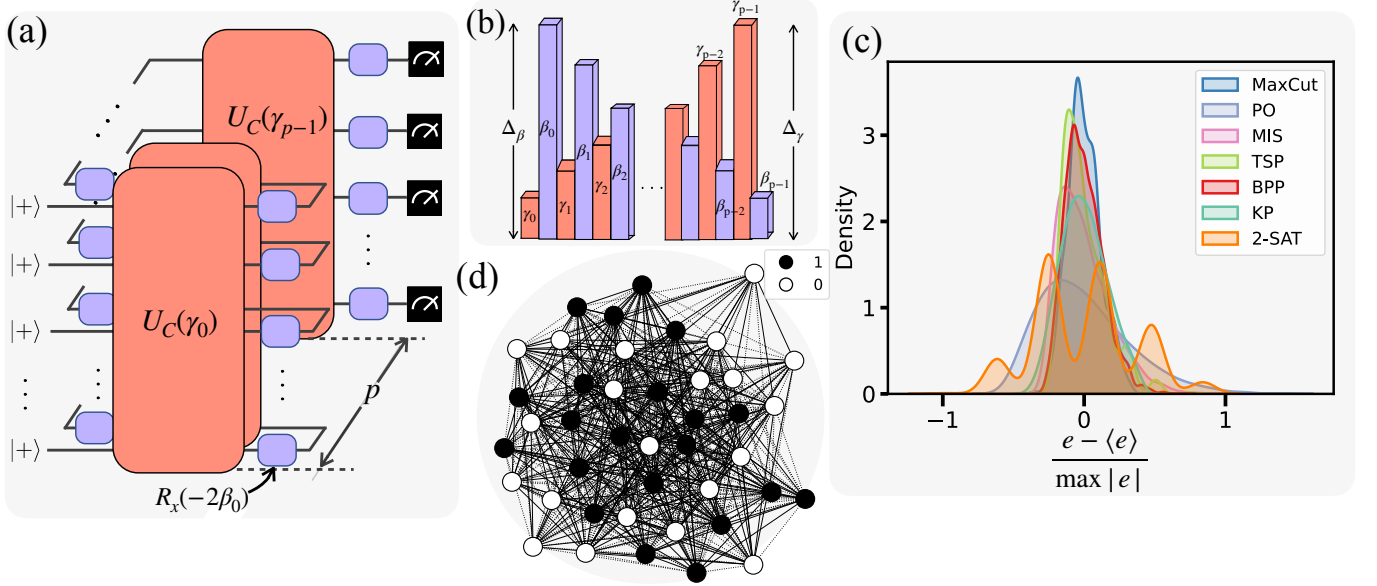


FIG. 1. (a) Quantum circuit of the QAOA algorithm, (b) LR-QAOA schedule, (c) eigenvalue distribution for the different COPs. All the distributions are for 10-qubit problems except BPP and TSP with 12-qubit and 9-qubit respectively. (d) An optimal solution for one of the 42-qubit W-MaxCut problems using $p = 50$ LR-QAOA. Dashed lines represent cuts, black (white) vertices qubits in 1 (0) state. At the end of the algorithm, the probability of finding the maximum cut is 32%.

changes the amplitude and direction of α_{000} using the information of this and the other states. The Hamming distance indicates how the amplitudes are grouped. For example, the effective vector $r_1 = (\alpha_{001} + \alpha_{010} + \alpha_{100})$ of states with Hamming distance 1, contribute to α_{000} after a $\pi/2$ rotation and a rescaling given by $\sin(\beta_t) \cos^2(\beta_t)$.

In Fig. 2(c) is shown the evolution of the optimal solution, x^* , of a 6-qubit W-MaxCut problem for the $U_C(\gamma_t)$ and $U_B(\beta_t)$ steps for $t \in \{0, \dots, Nq - 1\}$. In Fig. 2(d) shows the same evolution but for the lowest eigenvalue. In this case, the evolution of the eigenvalue due to $U_C(\gamma_t)$ goes in the opposite direction to the evolution of $U_B(\beta_t)$ producing the desired effect of interference. Fig. 2(e) shows the angle of rotation of the white triangles, i.e., the rotation due to $\theta(\gamma_t)$. The gain in the amplitude of the α_k^t at each time step after the unitary evolution $U_B(\beta_t)$ is shown in Fig. 2(f).

C. COPs

A detailed description of some COPs used in this work can be found in the appendix of [18]. We pick 5 random instances for different problem sizes. For the TSP, we use instances with 3, 4, 5, and 6 cities (9, 16, 25, and 36 qubits), where the distances between cities are symmetric and randomly chosen from a uniform distribution with values between 0.1 to 1.1. In the BPP, we consider scenarios involving 3, 4, 5, and 6 items (12, 20, 30, and 42 qubits). The weight of each item is randomly chosen from 1 to 10, and 20 is the maximum weight of the bins. The W-MaxCut, 3-MaxCut, MIS, KP, and PO problem

sizes are given by the number of qubits and chosen to be 4, 6, 8, 10, 12, 14, 16, 20, 25, 30, 35, and 40. For W-MaxCut and MIS we also include cases with 42 qubits.

For W-MaxCut problem simulations, we use randomly weighted edges with weights chosen uniformly between 0 and 1 and a probability of having an edge between any two vertices as 70%. One of these cases with its optimal solution is presented in Fig. 1(d). To test the conjecture about the linear time complexity of LR-QAOA, we use fully connected random W-MaxCut, MaxCut, Max-3-SAT, and Max-2-SAT problems. The weights for W-MaxCut are chosen from a uniform discrete distribution from 0 to 1000 in steps of 1. For random MaxCut problems, i.e., with a constant edge weight of 1, we vary the probability of having edges between nodes from 5% to 95%. We simulate 10 random problems from problem sizes between 15 to 35 qubits. For Max-2-SAT, we use 20 random instances up to 20 qubits and 10 random cases of Max-3-SAT with problem sizes between 15 to 25 qubits. A description of the Max-3-SAT problem setup is left in Sec. A 1. For MIS, edges between nodes are randomly selected with a 40% probability of having an edge. For KP problems, item values range from 5 to 63, weights from 1 to 20, and maximum weight is set to half of the sum of all weights. Finally, for PO, correlation matrix values are chosen from $[-0.1, 0, 0.1, 0.2]$, asset costs varying between 0.5 and 1.5, and the budget is set to half of the total assets cost.

For the inequality constraints in the KP, PO, and BPP, we use the unbalanced penalization approach [26, 28]. For the $probability(x^*)$ using unbalanced penalization, our focus is on finding the ground state of the cost Hamil-

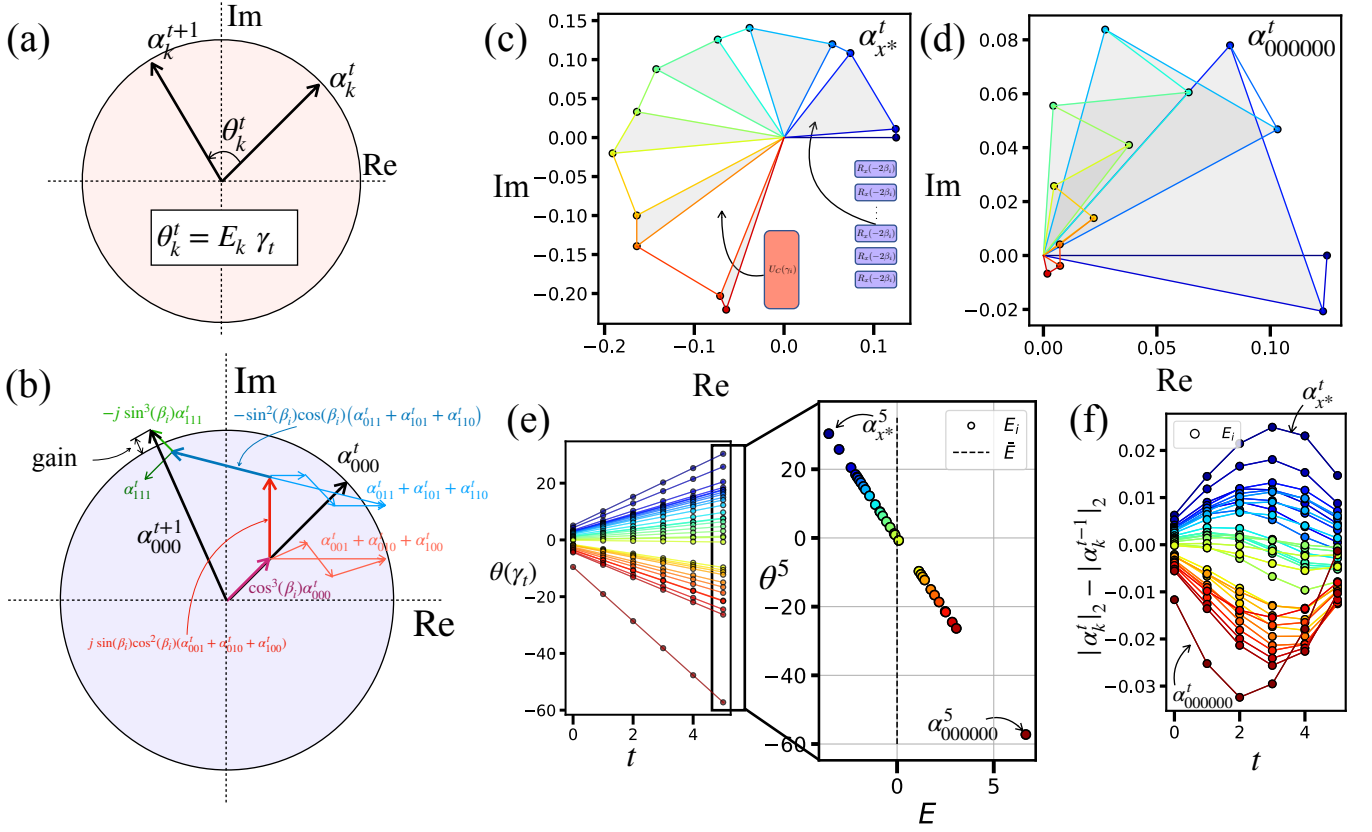


FIG. 2. LR-QAOA from the point of view of individual time steps. (a) The action of the $U_C(\gamma_t)$ gate on the state k at time step t , (b) evolution of the $|000\rangle$ amplitude after the application of $U_B(\beta_t)$ for a 3-qubit system, (c) evolution of the optimal solution, x^* , in a 6-qubit W-MaxCut problem. The gray (white) triangles are a time-step evolution due to $U_B(\gamma_t)$ ($U_C(\gamma_t)$). Line colors represent the time steps being blue (red) $t = 0$ ($t = 5$) step. (d) Evolution of the worst solution for the 6-qubit W-MaxCut problem. (e)-left LR-QAOA γ rotations at each layer for each state. Positive angles refer to counterclockwise rotations. Colors represent the energy of the state with darker blue (red) closer to the optimal (worst) solution of the problem. (e)-right last layer rotation in LR-QAOA vs. the energy, following Eq 7. (f) Amplitude gain evolution of the states after each $U_B(\beta_t)$ for the 6-qubit W-MaxCut problem.

tonian, since we are interested in knowing the LR-QAOA performance in finding the ground state of the Hamiltonian and there is no guarantee that the optimal solution of the original problem is encoded in the ground state of the Hamiltonian (see also the discussion in [26]).

We use the $probability(x^*)$ as a metric of the performance for the different COPs. Here, x^* represents the set of optimal bitstrings of the problem's Hamiltonian. Additionally, we use the approximation ratio for the MaxCut and its variations. The approximation ratio is given by

$$r = \frac{\sum_{i=1}^{N_q} C(x_i)/n}{C(x^*)}, \quad (10)$$

$$C(x) = \sum_{k,l>k}^{N_q} w_{kl}(x_k + x_l - 2x_k x_l), \quad (11)$$

where n is the number of samples, x_i the i th bitstring obtained from LR-QAOA, and $C(x)$ is the cost function of W-MaxCut, x^* is the optimal bitstring, $C(x^*)$ is the max-

imum cut, w_{kl} is the weight of the edge between nodes k and l , and x_k is the k th position of the x bitstring.

Figure 1-(c) presents examples of the eigenvalue distribution of the Hamiltonian for different COPs. In the scenario of large-scale problems, the distribution of eigenvalues tends to converge to a normal distribution [29].

D. Classical solvers

We compare LR-QAOA, SA [30], and CPLEX's spatial B&B [31] using TTS for the W-MaxCut problem. The TTS is given by

$$TTS = T \frac{\ln(1 - p_d)}{\ln(1 - probability(x^*))}, \quad (12)$$

where p_d is the target probability and T is the time complexity of the algorithm. For LR-QAOA, the time complexity comes from the number of layers used $T_{LR-QAOA} = p$ while for SA it comes from the number

of annealing steps and the number of transition states generated. We evaluate N_q transition states at every annealing step and therefore the time complexity for SA is $T_{SA} = SN_q$ where S is the number of annealing steps. We consider two strategies one with the number of steps constant $S = 5$ and another with the number of steps increasing linearly with the problem size $S = N_q$. For the case of B&B of CPLEX, for the sake of comparison, we consider the number of iterations to be the TTS.

E. Performance diagram

The performance diagram, introduced in [11], is a clear way to visualize the LR-QAOA performance. Figure 3-(a) shows the performance diagrams of a 10-qubit MIS problem. In the green-shaded 'annealing' region, LR-QAOA behaves like a continuous QA protocol. This region is delimited by small Δ and large p which guarantees yielding the optimal solution. The two points (black and white) marked in Fig. 3-(a) shows two LR-QAOA protocols with similar $probability(x^*)$. The white point is an LR-QAOA with $p = 300$ while the black point shows a LR-QAOA of $p = 17$.

In Fig. 3-(b), we present the performance diagram of a 10-qubit W-MaxCut using LR-QAOA. The shaded red region in this plot illustrates the 'ridge' as defined by [11]. The ridge region is characterized by consistently improving performance as the number of layers grows. The two points in this plot show similar performance, with the black point achieving a $probability(x^*) > 0.65$ with just $p = 20$, while the white point in the annealing region requires a higher $p = 300$.

F. Hamiltonian normalization

The Hamiltonian normalization is one important step in LR-QAOA. As we show, every eigenvalue rotates accordingly to Eq. 7, which means that the normalization limits the rotation angle fixing the *ridge region* to a specific location in the performance diagram. The general form of the COP's Ising Hamiltonian is given by

$$H_c(z) = \frac{1}{\max\{|J_{ij}|\}} \left(\sum_{i=0}^{n-1} \sum_{j>i}^{n-1} J_{ij} z_i z_j + \sum_{i=0}^{n-1} h_i z_i + O \right), \quad (13)$$

where J_{ij} and h_i are real coefficients that represent the COP, and the offset, O , is a constant value. Since O does not affect the location of the optimal solution, it can be left out for the sake of simplicity. There are different ways of normalizing the Hamiltonian, we identify two, normalizing by $\max\{|J_{ij}|\}$ or $\max\{|h_i, J_{ij}|\}$, and use them on each problem. We select the one with the best results in terms of $probability(x^*)$. We find that the $\max\{|J_{ij}|\}$ strategy improves faster the $probability(x^*)$ while $\max\{|h_i, J_{ij}|\}$ improves optimal

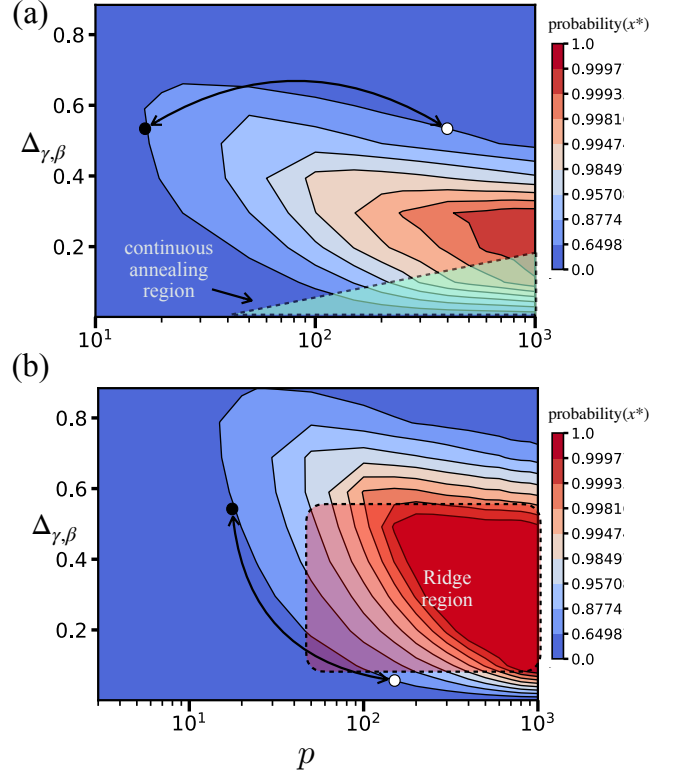


FIG. 3. Performance diagram using LR-QAOA on (a) a 10-qubit MIS and (b) a 10-qubit W-MaxCut problem. The y-axis represents $\Delta_{\gamma,\beta}$, and the x-axis is the number of LR-QAOA layers. The colors represent the $probability(x^*)$ landscape, i.e., the probability of finding the optimal solution with darker red approaching the 100%. Circles in white and black represent similar $probability(x^*)$ cases. The arrows connecting them are guiding elements.

and suboptimal energies. For the results presented, we choose to normalize the Hamiltonian by $\max\{|J_{ij}|\} \forall i > j \in 0, \dots, n-1$ for almost all the cases except MIS where we use $\max\{|h_i|\} \forall i \in 0, \dots, n-1$.

Mitigation: Hamming distance 1

In [18], we introduce the mitigation technique used here. This involves applying a bitflip to each position within the output bitstring of samples from a quantum computer, to mitigate single-qubit bitflips. The computational overhead of this postprocessing method is $O(NN_q)$, where N represents the number of samples and N_q is the number of qubits. The success of this method relies on the large probability LR-QAOA of amplifying solutions close to the optimal. The details of our proposed approach are described in Algorithm 1.

Algorithm 1: Sampler mitigation

Data: bitstring samples $S = [s_0, \dots, s_{N-1}]$
Result: Samples corrected S_{mitig}

Initialization;

```

for  $i=0; i++; i < N$  do
   $E_{best} = \text{Energy}(S[i]);$ 
   $s_{best} = S[i];$ 
  for  $j=0; j++; j < N_q$  do
     $s_{new} = S[i];$ 
    if  $s_{new}[j] == 1$  then
       $s_{new}[j] = 0$ 
    else
       $s_{new}[j] = 1$ 
     $E_{new} = \text{Energy}(s_{new});$ 
    if  $E_{new} < E_{best}$  then
       $E_{best} = E_{new};$ 
       $s_{best} = s_{new};$ 
   $S_{mitig} \leftarrow s_{best}$ 
return  $S_{mitig};$ 

```

G. Experimental details

We implement W-MaxCut problems using LR-QAOA with $\Delta_\gamma = 0.6$ and $\Delta_\beta = 0.3$ on three quantum computing technologies: IonQ Aria a fully connected 25-qubit device based on trapped ions with 2-qubit gate error of 0.4% and 2-qubit gate speed of $t_{2q} = 600\mu s$ [32], labeled *ionq_aria*, Quantinuum H2-1 (a fully connected 32-qubit device based on trapped ions with a 2-qubit error rate of 0.2% [24], labeled *quantinuum_H2*), and three IBM Eagle superconducting processors [33], 127 transmon qubits with heavy-hex connectivity and 2-qubit median gate error between 0.74 and 0.95%, error per logical gate (EPLG) [34] between 1.9% and 3.6%, and 2-qubit gate speed of $t_{2q} = 0.66\mu s$, labeled *ibm_brisbane*, *ibm_kyoto* and *ibm_osaka*).

We perform different experiments to assess the practical performance of quantum technology to solve COPs using LR-QAOA. First, an experiment on *ionq_aria* for a 10-qubit W-MaxCut with 70% of random connections as described in Section II C, this helps for the sake of comparison with a depolarizing noise model, Fig. 7. Additionally, different problems from 5 to 109 qubits were tested on *ibm_brisbane* using a W-MaxCut problem with a 1D-chain topology shown in Fig. 9-(a). We opt for a simple graph due to constraints posed by noise. Additionally, we provide an experimental comparison across three distinct IBM devices for a 109-qubit W-MaxCut problem. Finally, a comparison between *ionq_aria*, *ibm_brisbane*, and *quantinuum_H2* is shown for a 25-qubit W-MaxCut problem, Fig. 9-(b).

The time of execution t_e for 1D chain topology LR-QAOA protocol can be approximated to that of the 2-qubit gates. This is because single-qubit operations are a minority and their execution time is generally faster than 2-qubit gates. In *ionq_aria* the 2-qubit gates are

executed sequentially so $t_e = t_{2q}N_{2q}p$ where N_{2q} is the number of 2-qubit terms in the cost Hamiltonian. For the case of *ibm_brisbane*, the time of execution is $t_e = 2t_{2q}p$. *quantinuum_H2* can execute 4 2-qubit gates in parallel, hence, the execution time is $t_e = t_{2q}(N_{2q}/4)p$. The time per 2-qubit gate is $600\mu s$ on *ionq_aria*, and $660ns$ on *ibm_brisbane*. We could not find information about t_{2q} for *quantinuum_H2*, but we assume it is similar to *ionq_aria*. Therefore, a 25-qubit W-MaxCut with 1D topology requires $14.4ms$, $3.6ms$, and $1.32\mu s$ for each layer using *ionq_aria*, *quantinuum_H2*, and *ibm_brisbane*, respectively. For each experiment on IBM devices, *ionq_aria*, and *quantinuum_H2* we use 10000, 1000, and 50 samples, respectively.

H. Noise model

At the instruction level, the main source of noise in digital quantum computers comes from the 2-qubit entangling gates [35]. Thus, we use a depolarizing noise channel in the 2-qubit gates of the LR-QAOA protocol. This channel is given by

$$\mathcal{E}[\rho] = (1 - \lambda)\rho + \lambda \frac{I}{4}, \quad (14)$$

where λ is the depolarizing error parameter, I is a 4×4 identity matrix, and ρ is the density matrix of the 2-qubit system. In general, the action of a 2-qubit gate on a general density matrix can be expressed by

$$\mathcal{E}_{ij}[\rho] = (1 - \lambda)U_{2Q}^{ij}\rho U_{2Q}^{ij\dagger} + \frac{\lambda}{4}\text{Tr}_{ij}(\rho) \otimes I, \quad (15)$$

where \mathcal{E}_{ij} is the channel acting on ρ , Tr_{ij} is the partial trace over qubits i and j , and U_{2Q}^{ij} is the 2-qubit unitary gate. For simplicity, we assume λ is the same for all the 2-qubit gates.

III. RESULTS
A. Simulations

Figures 4-(a)-(d) show the probability of success for different COPs vs. the number of qubits. We test problems with 4 to 42 qubits using the LR-QAOA with $p = 10$ to 400, $\Delta_\gamma = 0.6$, and $\Delta_\beta = 0.3$. The error bars represent the minimum and maximum *probability*(x^*) over 5 random cases and the circles are the mean value. The colors represent the number of layers p used. Figure 1-(d) shows one of the 5 random cases of W-MaxCut with 42-qubit of Fig. 4-(a). In this example just employing 50 layers of LR-QAOA results in an amplification of 12 orders of magnitude in the probability of success from approximately $2/2^{42} \approx 4.54 \times 10^{-13}$ to 0.32. To provide context, if we were to solve the same task using Grover's algorithm [36], it would require approximately

$\sqrt{2^{42}}/2 \approx 2 \times 10^6$ iterations of the oracle, along with the diffuser. The dashed lines in Figs. 4-(a)-(d) are added as guiding lines. They represent $1/2^{(\eta N_q/p)}$ where η is a constant. The η values used are (a) $\eta = 2.8$, (b) $\eta = 4$, (c) $\eta = 2.5$, and (d) $\eta = 3.5$. These results suggest that the $probability(x^*) = 1/2^{(\eta N_q/p)}$ for the random instances of different COPs analyzed. The implications are significant, for example, increasing the number of layers proportional to the number of qubits, i.e. $p = N_q$, one should observe that the probability of success must remain constant. We test if this is the case, in the Sec. IIIB.

Figure 4-(e) shows the probability of success for different combinatorial optimization problems up to 42 qubits using the LR-QAOA protocol with $p = 100$. The dashed line, $1/2^{N_q/2}$, is added as a guiding line, it reflects a quadratic speedup in the search space. The best performance is obtained for W-MaxCut with an average $probability(x^*) = 0.58$ at 40 qubits which compared to the optimal solution initial amplitude $2/2^{40} \approx 0.18 \times 10^{-11}$ is an 11 orders of magnitude increment in only 100 layers of LR-QAOA. The lowest performance is for the TSP and BPP; for example, for a 6 cities problem (36 qubits) we get an average $probability(x^*) = 0.15$ which compared with the random guessing probability $1/2^{36} \approx 0.145 \times 10^{-10}$ is a gain of 10 orders of magnitude. However, it is worth noting, that the number of feasible solutions to this problem is $(cities - 1)!/2 = 60$, resulting in a random guessing probability within the feasible space of approximately $1/60 \approx 0.0166$.

Figure 4-(f) shows the average performance of LR-QAOA for the W-MaxCut problem in terms of the fractional error $1 - r$ vs. the number of qubits, where r is the approximation ratio given by Eq. (10). The maximum number of qubits used is 40. Different colors represent the number of layers from 10 to 400. As expected, an increase in the number of layers leads to an increase in the average performance of LR-QAOA to find better solutions. Additionally, the relation of $1 - r$ tends to stay constant with an increment in the number of qubits; this aligns with the minimum performance guarantee of MaxCut for a fixed number of QAOA layers [37].

Figure 4-(g) shows a 12-qubit PO probability vs. the cost of the first 3000 sorted eigenvalues using LR-QAOA from 10 to 200 layers. The dots represent the probability of getting a certain cost Hamiltonian eigenvalue vs. the cost associated with it. Only the first 3000 eigenvalues with the lowest cost are presented. This plot shows another characteristic of LR-QAOA, namely that the probability of obtaining a given solution drops exponentially with increasing cost. Even if the optimal solution is not observed in one sample of LR-QAOA, it is more likely that a low-cost energy is observed.

B. Conjecture

To add further evidence that $probability(x^*) = 1/2^{(\eta N_q/p)}$, we simulate LR-QAOA for fully connected W-MaxCut random problems for 100 cases and problem size ranging from 5 to 42 qubits using $p = N_q$. In Fig. 5, we show evidence supporting this hypothesis.

Figure 5-(a) shows the $probability(x^*)$ for different problem sizes. The dots represent the probability of success for individual cases and the black circle is the mean value for a $\Delta_{\gamma,\beta} = 0.5$. After reaching $N_q = 25$, there is a decline in performance using $\Delta_{\gamma,\beta} = 0.5$. To address this, we adjust $\Delta_{\gamma,\beta}$ to 0.4 for certain problem sizes, which leads to an improvement in performance. The data points corresponding to $\Delta_{\gamma,\beta} = 0.4$ are shown with triangles. This suggests that one must reduce $\Delta_{\gamma,\beta}$ as the number of qubits increases. Interestingly, maintaining $N_q = p$ does not result in any significant performance loss. This observation strengthens the hypothesis that $probability(x^*) = 1/2^{(\eta N_q/p)}$. If this relation were to hold, it would mean that LR-QAOA is a polynomial time quantum algorithm for solving general instances of NP-Hard problems. However, it is still possible that there is a mild exponential decay for this problem that cannot be noticed at ≤ 42 qubits. Even if this is the case, a scaling advantage is plausible.

Figure 5-(b) shows the approximation ratio for the same problems of (a). The decrement in performance is more notorious in terms of the approximation ratio for $\Delta_{\gamma,\beta} = 0.5$. The modification of $\delta_{\gamma,\beta} = 0.4$ leads to a general improvement in terms of the quality of the solutions. It has been proven by Theorem 4.2 in [38], that it is NP-Hard to approximate MaxCut for a factor of $16/17 \approx 0.941$. The dashed line represents $r = 0.878$, the Goemans and Williamson (GW) algorithm [39], which is the best-known polynomial-time algorithm and according to the unique games conjecture also the best possible polynomial-time algorithm for this problem [40, 41].

Figure 5-(c) shows the $TTS_{99\%}$ for a $p_d = 0.99$ in Eq. 12 of the W-MaxCut problems for SA and LR-QAOA. We include the CPLEX number of iterations needed to find the optimal solution for comparison. This plot shows the exponential scaling of classical solvers to find the optimal solution to NP-hard problems. On average, it grows with $N_{iterations} = 2^{0.38N_q+1.5}$ for CPLEX after 20 qubits. In the case of LR-QAOA, it stabilizes at around 10^3 iterations, and at $N_q = 42$, it has improved by two orders of magnitude the TTS compared to SA. LR-QAOA has the fundamental advantage of knowing the full energy spectrum of the COP at each time step while the other methods need some time to learn it.

Fig. 5-(d) shows some instances of Max-2-SAT (triangles) and Max-3-SAT (circles) problems. The Max-3-SAT 10 random instances for problem sizes up to 25 qubits are chosen from a ratio of clauses/variables = 4.16 which is close to the critical region where the problems are known to be hard to solve [42, 43]. In this case, the relation $probability(x^*) = 1/2^{\eta N_q/p}$ seems to be valid on

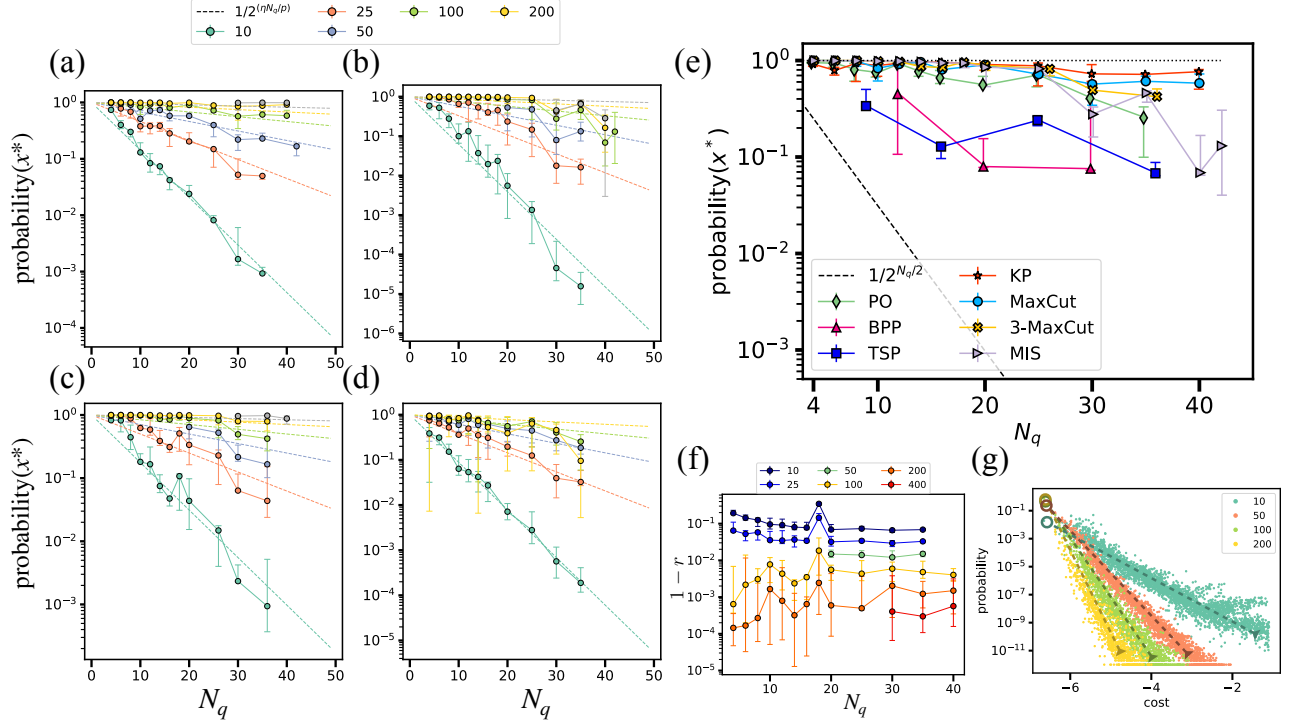


FIG. 4. Probability of success for 5 random instances of (a) W-MaxCut, (b) MIS, (c) 3-MaxCut, and (d) PO. The error bars represent the minimum and maximum over the 5 cases. The different colors represent the number of LR-QAOA layers (see legend). Dashed lines represent the conjectured scaling $1/2^{(\eta N_q/p)}$ for each p . (e) Probability of success for 5 random instances for different COPs using a $p = 100$ LR-QAOA. Markers represent the median value and error bars represent the Q1 and Q3 quartiles. The average performance of LR-QAOA as measured by (f) the fractional error, $1 - r$, of the instances of W-MaxCut from (a), and (g) probability vs. cost of an instance of a 12-qubit PO solved using LR-QAOA with different p from 10 to 200.

the average case. The Max-2-SAT problems used are obtained from a dataset of hard instances of this problem for SA and QA [44]. What makes these problems special is the number of degeneracies of the first excited state. For example, in the inset of this figure, it is shown a 20-qubit case. The optimal solution has 2 degeneracies while the first excited state has 6516. This causes SA and QA to get stuck in solutions close to optimal ones. In our case, LR-QAOA with $p = N_q$ does not hold a constant probability of success, so we can expect that $\text{probability}(x^*) = 1/2^{\eta N_q/p}$ relation does not hold always.

Fig. 5(e) shows the LR-QAOA $p = N_q$ probability of success for 10 random cases of the MaxCut for up to 35 qubits. We use 7 different problems of MaxCut that we classify depending on the percentage of edges of the graph. The colors represent the average number of edges in the graph, meaning 0.05 having 5% of all possible edges (dark blue) and 0.95 a 95% of all possible edges (dark red). In this case, on average the $p = N_q$ seems to hold $\text{probability}(x^*) = 1/2^{\eta N_q/p}$. However, the worst case highlighted with the red circle deviates considerably from the average performance. We explore this case and find the same characteristic that makes Max-2-SAT hard for LR-QAOA, a high degeneracy close to the optimal so-

lution. Finally, Fig. 5(f) shows the number of iterations needed to solve the same MaxCut problems of Fig. 5(e) using CPLEX. In this case, it is classically hard to find the optimal solution for densely connected graphs with a worse-than-quadratic speedup for edge probabilities from 80% to 95%.

With this extra information at hand, we present the following conjecture.

Conjecture 1. For a given COP solved using LR-QAOA, there is a $\Delta_{\gamma,\beta}$ for which the probability of finding the optimal solution scales according to $\text{probability}(x^*) = 1/2^{(\eta N_q/p)}$ for a constant η , p LR-QAOA layers, and N_q qubits, iff there is no high concentration of solutions near the optimal solution.

This conjecture is helpful as a first attempt to know the expected performance of LR-QAOA for a given problem. It may suggest that LR-QAOA can find solutions to general instances of NP-Hard problems in polynomial time. However, the evidence involves solutions of a limited size and it is still possible that there is a mild exponential decay for problems like W-MaxCut. In the case of problems with suboptimal solutions densely concentrated close to the optimal, there is a noticeable exponential decay for $p = N_q$. In this scenario, for instance, in the Max-2-SAT problem, LR-QAOA still gives a quadratic speedup. In

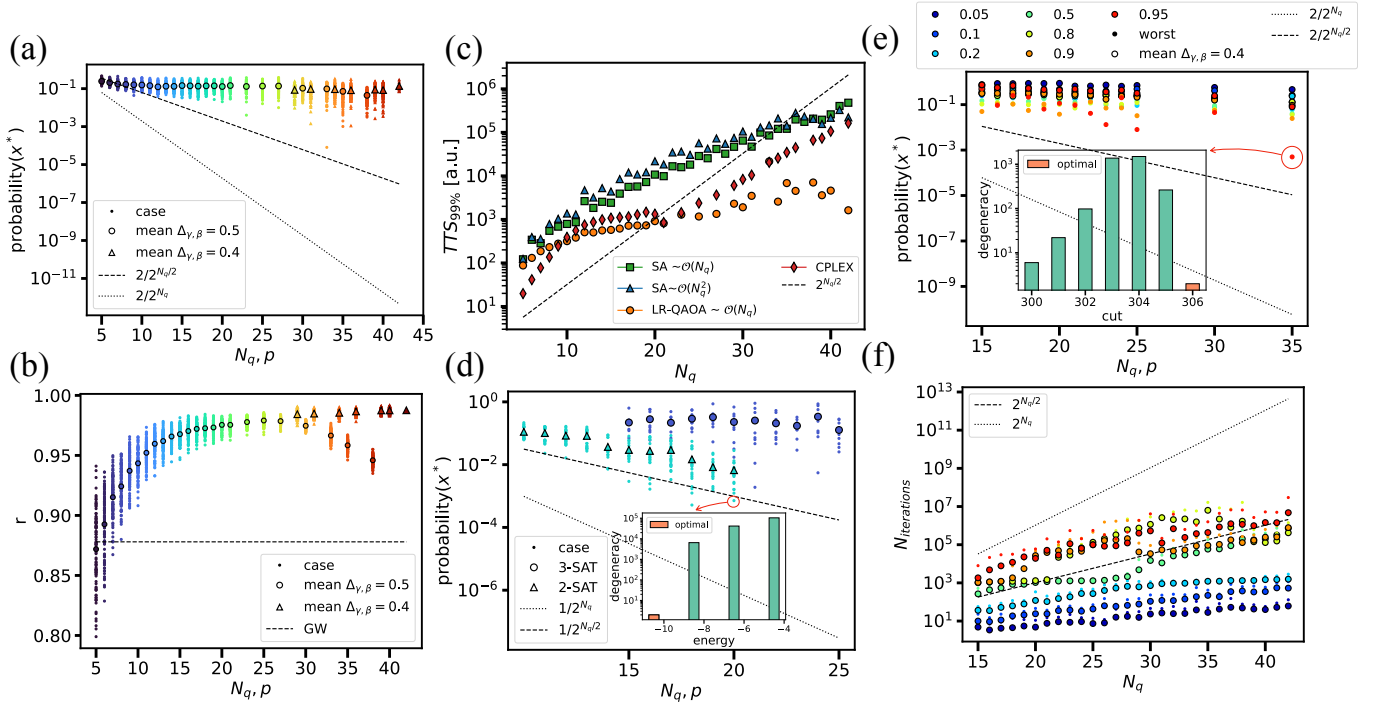


FIG. 5. Evidence for conjecture 1. The problems shown here are solved using LR-QAOA with $p = N_q$ (a) Probability of success of fully connected W-MaxCut problem using 100 random W-MaxCut problems up to 40 qubits and 10 problems for 42 qubits. The different vertically stacked dots represent individual cases and the circles (triangles) indicate the mean value $\Delta_{\beta,\gamma} = 0.5$ ($\Delta_{\beta,\gamma} = 0.4$). The dotted line represents the probability of finding the optimal solution by random guessing and the dashed line represents the probability of finding the optimal solution if the search space is reduced by a quadratic speedup algorithm. (b) Approximation ratio for the W-MaxCut problems. The dashed line (GW) represents the approximation ratio using the best-known polynomial-time classical algorithm for the same problem. (c) TTS for SA and LR-QAOA compared to CPLEX's number of iterations. The dashed line is added as a guiding line it represents a quadratic speedup $2^{N_q/2}$. (d) 20 hard cases of Max-2-SAT problems (triangles) for problem sizes up to 20 qubits and 10 random cases of Max-3-SAT problems (circles) for problems up to 25 qubits. The inset shows the degeneracies of the 4 first eigenvalues for the Max-2-SAT problem highlighted in red. (e) 10 random MaxCut instances for problem sizes up to 35 qubits. The different colors mean the average percentage of edges compared to a fully connected graph. Therefore, darker blue, 0.05, means a 5% of having edges. The circles represent the mean value and the dots represent the worst case. The inset shows the degeneracies of the solutions in the worst case. (f) The number of iterations needed to find the optimal solution using CPLEX for the MaxCut problems. The colors follow the same pattern as in (e).

this case, the high degeneracy causes the dense concentration of solutions close to the optimal one. Similarly, in the TSP or BPP, the concentration of solutions occurs due to penalization terms concentrating the valid solutions space on a small region. We suspect that in the limit, i.e., a random oracle with only one ground state and the first excited state containing all other possible solutions, like the one in [45], one would need $p = 2^{\eta N_q}$ layers to amplify the solution to some threshold for a constant η , similar to the performance guarantee in Grover's algorithm.

C. Experiments

In this section, we show numerically and experimentally how noise affects LR-QAOA. Before moving to numerical simulations of LR-QAOA under depolarizing

noise, we want to show LR-QAOA's ability to correct errors along the way. In Fig 6-(a), the noiseless evolution of the eigenvalues of the cost Hamiltonian for LR-QAOA is presented. In Fig.6-(b) the same protocol is shown but this time depicts the evolution under full inversion of the qubits using a layer of X gates applied at $p = 15$. At $p = 16$, the eigenvalues experience a full inversion of probabilities with high energy bitstrings now having a large probability. This is quickly corrected by LR-QAOA increasing the probability of getting the optimal solution. This inversion comes with the price of a reduction in the success probability from 96.1% in (a) to 28.5% in (b).

Figure 7 shows 10-qubit W-Maxcut problem results using LR-QAOA and depolarizing noise for λ s of Eq. 14 from 10^{-1} to 10^{-5} affecting only the 2-qubit gates. We compare these results with the ones obtained using *ionq-aria* (diamonds) for the same problem. Fig. 7-(a) shows how the probability of success vs. the num-

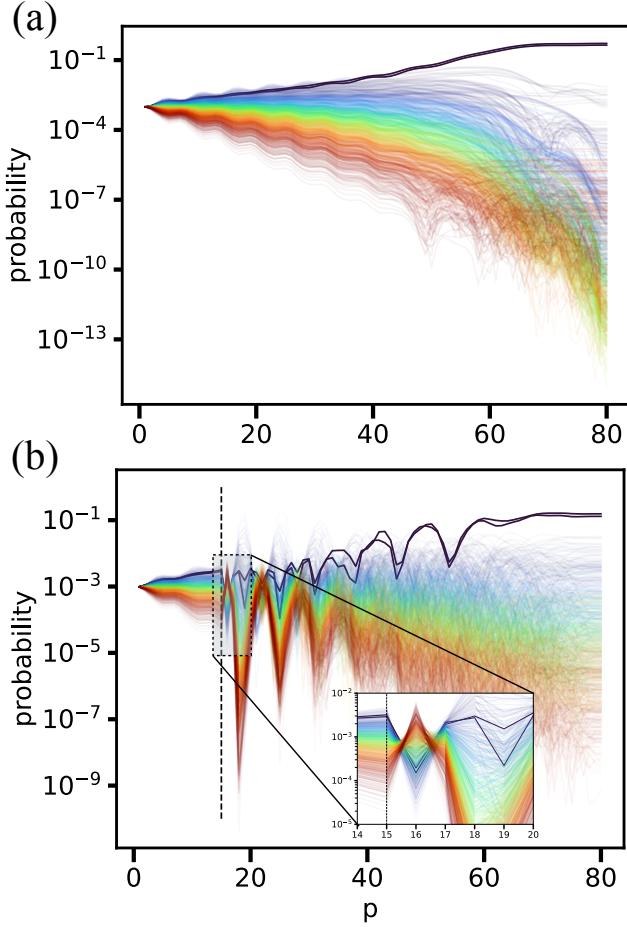


FIG. 6. Probability of observing the different bitstring solutions of a 10-qubit MIS problem for the LR-QAOA protocol with $p=80$ (a) noiseless evolution (b) a layer of X gates applied at $p=15$. The lines on the graph represent various eigenvalues, with darker blue indicating lower energy and darker red indicating higher energy. The two values highlighted in dark blue correspond to the optimal solutions for the given problem.

ber of LR-QAOA layers for the different depolarizing noise strengths. Fig. 7-(b) shows the approximation ratio vs. the number of LR-QAOA layers for the same problem. In both plots, *ionq-aria* results agree with a $\lambda = 6 \times 10^{-4}$. Finally, Fig. 7-(c) shows the maximum probability of success vs. λ . At $\lambda > 5 \times 10^{-2}$ information can still be recovered and at $\lambda = 10^{-5}$ errors are so slowly added that the algorithm can in some sense correct them, similar to what we show in Fig. 6-(b).

Figure 8-(a) shows the probability of success vs. the number of LR-QAOA layers of random cases of the W-MaxCut for variables from 5 up to 30 running on *ibm.brisbane*. We use 10000 samples for each problem size. We do not include information for larger problem sizes because no optimal solution is observed for them. The dashed line represents the probability of success of mitigated samples of a random sampler. In other words,

circles above the dashed line of its respective color cannot be explained as the result of a random process and therefore can be attributed to LR-QAOA. To contextualize our outcomes, observing the optimal solution for the 30 qubits problem with a random sampler requires in the worst case $2^{30}/2 = 536.870.912$ evaluations of the cost function. In our experiment, we find the optimal solution 2 times at 13 layers using LR-QAOA on a noisy device using 10000 samples and the mitigation technique. This means 10000×30 further evaluations representing an improvement over random guessing of $536.870.912/310.000 \approx 1732$ times.

Figure 8-(b) shows the approximation ratio of the instances of W-MaxCut from 5 to 109 qubits using LR-QAOA on *ibm.brisbane*. The vertical dashed line at $p = 10$ indicates the number of layers for which the best performance of LR-QAOA is obtained. After $p = 10$, the system is slowly moved towards a maximally mixed state. At $p = 100$, it is reached in all the cases. We attribute this phenomenon to the characteristics of LR-QAOA to correct errors on the way. This leads to an interesting behavior, for instance, at $p = 3$ the approximation ratio is the same as that at $p = 40$ for the 109-qubit case, despite the latter requiring roughly 13 times more time and 2-qubit gates than the former.

Figure 8-(c) shows the maximum probability over all layers vs. the number of qubits for the 1D W-MaxCut experiment. The dashed line that represents the quadratic speedup $1/2^{N_q/2}$ is added as a reference. In the experiments, the highest probability occurs within the range of $p = 10$ to 13. The experiments hold a similar decay to the quadratic speedup, with a shift that can be attributed to the mitigation technique. Additionally, Fig. 8-(d) shows the best approximation ratio among all the samples vs. the number of qubits. The maximum average approximation ratio for the 109-qubit experiment is $r = 0.64$ with the best sample having a $r = 0.84$.

Figure 9-(a) shows the approximation ratio of the 109 qubits W-MaxCut problem using LR-QAOA from $p = 3$ to $p = 100$. At $p = 10$, the maximum approximation ratio is reached for the three devices *ibm.brisbane*, *ibm.kyoto*, and *ibm.osaka*. The noise at larger p leads the system towards a maximally mixed state, so we include the dashed line that represents the approximation ratio $r = 0.5326$ of a random sampler after the mitigation technique is applied. Unexpectedly, at $p = 100$, results for *ibm.kyoto* and *ibm.osaka* still deviate from the random sampler and therefore some information of the LR-QAOA protocol is present. The circuit used requires 21200 CNOT gates and a total time of $\approx 132\mu s$. This is an indication of the resilience of the LR-QAOA to noise.

At this scale, we surpass the point where exact classical simulation of LR-QAOA is feasible both in terms of the number of qubits and depth of the circuit. Therefore, we believe that this experiment can be presented as a quantum supremacy/utility experiment. This means that a classical algorithm cannot mimic the sampling properties of LR-QAOA at large p and N_q . There are differ-

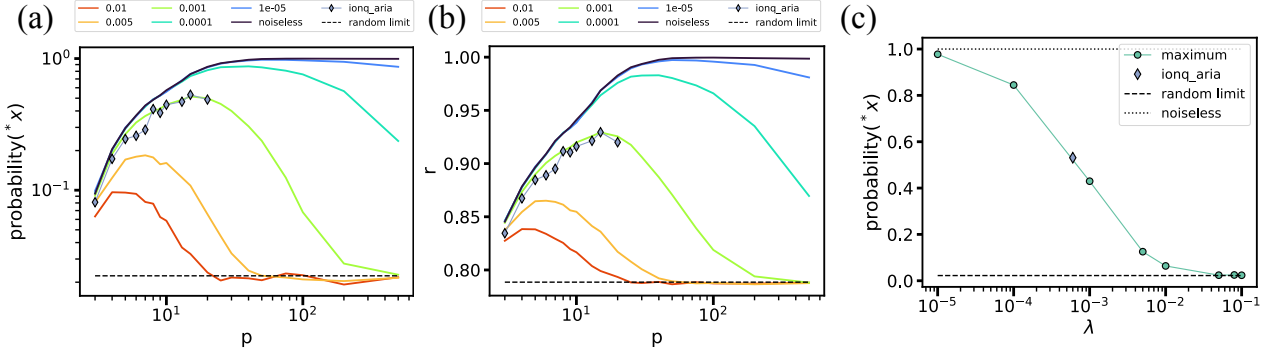


FIG. 7. Results of LR-QAOA for the 10-qubit random W-MaxCut problem at different p when noise is added at different depolarizing noise strength λ . (a) probability of success (b) approximation ratio (c) largest probability of success for each λ . Diamonds represent the same problem executed on *ionq_aria*. Different lines represent the strength λ of the depolarizing channel. The shaded line shows the probability of obtaining the optimal solution by random guessing.

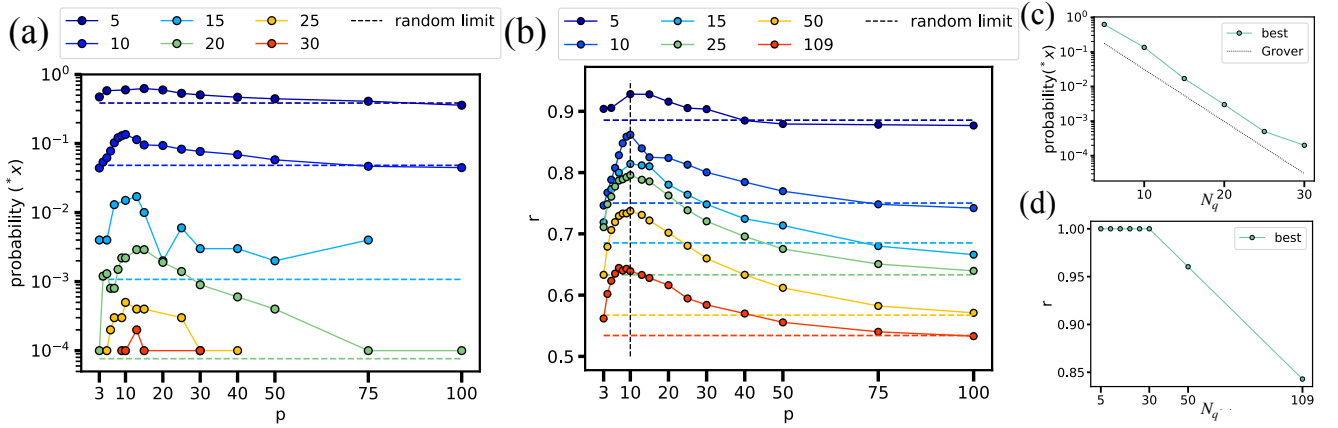


FIG. 8. Experimental results of the LR-QAOA protocol on *ibm_brisbane* for W-MaxCut problems. (a) Probability of success vs. number of layers of the LR-QAOA protocol. Colors represent the number of qubits from 5 to 30 qubits. The dashed lines 'random limit' represent the success probability of a random sampler after the mitigation technique is applied for each problem with the same color. (b) Approximation ratio vs. LR-QAOA layers. Colors represent problems from 5 to 109 qubits. (c) Best probability of success of (a) vs. number of qubits. The dashed line representing a quadratic speedup is added as a reference. (d) Best approximation ratio of all the samples in the experiment vs. number of qubits.

ent techniques proposed for addressing the simulation of quantum supremacy [46] or utility [47] experiments after their publication (e.g., [48, 49]), so the validation of this remains subject to evaluation within the research community. Independently of the answer, these results indirectly imply the efficacy of LR-QAOA to solve COPs in scenarios involving more than 42 qubits.

Figure 9-(b) presents a comparative analysis between *ionq_aria*, *quantinuum_H2*, and *ibm_brisbane* in solving a 25-qubit instance of the W-MaxCut problem. The number of samples is 10000 for the noiseless simulator and *ibm_brisbane*, 1000 for *ionq_aria*, and 50 for *quantinuum_H2*. The performance of *quantinuum_H2* stands out, achieving a maximum approximation ratio of $r = 0.95$ at $p = 50$, compared to $r = 0.98$ at $p = 50$ of the noiseless simulator, *ibm_brisbane*'s $r = 0.80$ at $p = 10$, and *ionq_aria* $r = 0.90$ at $p = 10$.

From a time perspective, executing an instance of W-

MaxCut LR-QAOA for $p = 10$ on *ibm_brisbane* requires approximately $\approx 13.2\mu s$, whereas *ionq_aria* completes the same task in about $\approx 144ms$, and *quantinuum_H2* in $\approx 36ms$. The three devices successfully identify the optimal solution for this problem, with *quantinuum_H2* achieving a maximum probability of success of 0.10 at $p = 75$, *ionq_aria* achieving a maximum probability of success of 0.008 at $p = 10$, and *ibm_brisbane* reaching 0.0005 at $p = 10$. This means that *quantinuum_H2* is 12.5 times more effective in finding the optimal solution than *ionq_aria*, and 200 than *ibm_brisbane*.

However, the accuracy gain for *quantinuum_H2* does not fully compensate for the time required for sampling. In other words, for every optimal sample obtained from *quantinuum_H2*, one could obtain approximately 2700 samples on *ibm_brisbane*. To observe an optimal solution at $p = 10$ using *ibm_brisbane* we need $\approx 13.2 \times 10^{-6} / 0.0005 = 0.0264s$ while *quantinuum_H2*

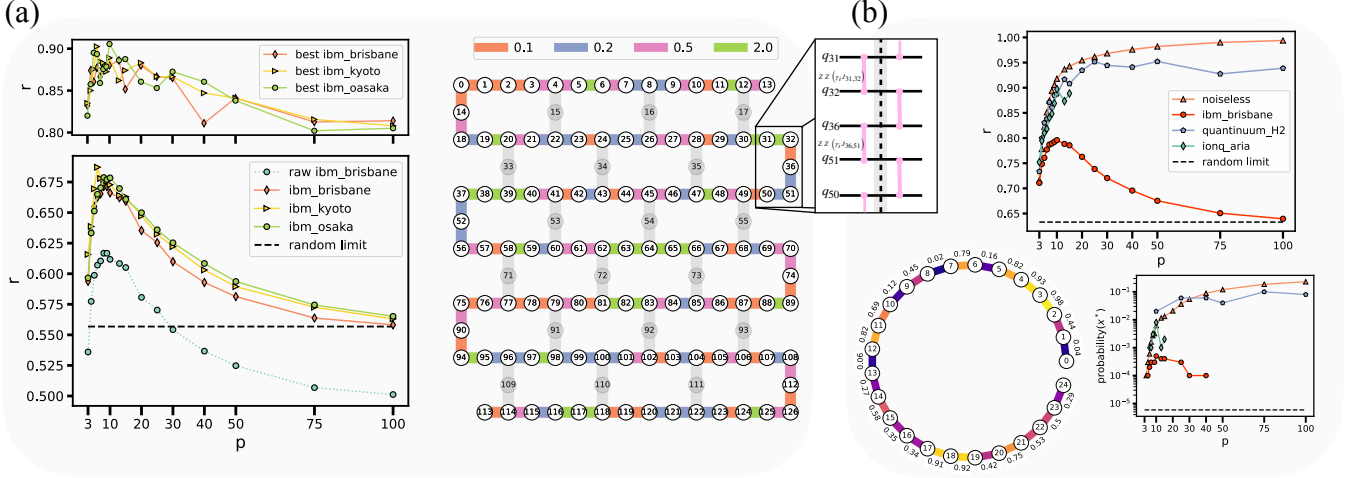


FIG. 9. (a) 109-qubit W-MaxCut experiment on IBM Eagle devices using LR-QAOA. The upper-left plot represents the best approximation ratio observed from the 10000 samples at each p . The bottom-left plot shows the average approximation ratio where the dotted line represents the raw result from *ibm_brisbane* and the solid lines represent the mitigated results over the three different IBM devices. The black dashed line is the limit where the system reaches the maximally mixed state. The right plot shows the IBM Eagle layout with the 1D random W-MaxCut on it. The colors represent the random weights chosen from 4 possible values 0.1, 0.2, 0.5, and 2.0 for each edge in the graph. The inset shows how the 2-qubit gates are implemented using only a depth of 2 for each LR-QAOA layer. (b) 25-qubit W-MaxCut experiment comparative analysis for 3 different vendors. The bottom-left plot presents the graph of the W-MaxCut selected with the corresponding weight values. In the upper plot, the approximation ratio of the devices with the triangles, circles, diamonds, and pentagons correspond to the mitigated results from a noiseless simulation, *ibm_brisbane*, *ionq_aria*, and *quantinuum_H2*, respectively. Because of a limitation in the maximum number of single-qubit and two-qubit gates, there are no results above $p = 15$ using *ionq_aria*. In the bottom left plot the probability of success for the same experiment.

$\approx 36 \times 10^{-3} / 0.02 = 1.8s$. This means when *quantinuum_H2* finds a solution, *ibm_brisbane* has already found 68.

IV. CONCLUSIONS

In this work, we have presented analytical, numerical, and experimental evidence that LR-QAOA constitutes a universal QAOA protocol. This means that this protocol works efficiently independently of the problem tested, increasing the probability of success as the number of layers increases. We simulate MIS, BPP, TSP, MaxCut, W-MaxCut, 3-MaxCut, KP, PO, Max-2-SAT, and Max-3-SAT problems with up to 42 qubits and 400 layers on the modular supercomputer JUWELS [20]. Additionally, we test LR-QAOA using W-MaxCut problems from 5 to 109-qubit cases and p from 3 to 100 on real quantum hardware using *ibm_brisbane*, *ibm_osaka*, *ibm_kyoto*, *quantinuum_H2*, and *ionq_aria* finding that LR-QAOA is resilient to noise. We show that this characteristic comes from the algorithm's ability to overcome noise. While noise pushes the system through a maximal mixed state, LR-QAOA pushes to a minimum energy correcting errors on the way.

One important conclusion from this work is that one can completely suppress the classical optimization step in QAOA. With the fixed schedule in LR-QAOA, one

can inexpensively jump to the number of layers needed to observe the optimal solution within a given number of samples.

We show the evolution of LR-QAOA from the perspective of the amplitudes of the computational basis states. This change in framework allows us to explain the evolution of the amplitudes under the application of U_C and U_B . Under the application of U_C , each amplitude is rotated proportionally to the state energy. The case of U_B is more complex but every amplitude evolves with contributions from the other states' amplitude with the Hamming distance as the indicator of how to group their contribution. The annealing characteristics of LR-QAOA along with a constant rotation of the states' amplitude (constant slope of the linear ramp) under U_C allow the exploitation of an interference pattern that enhances the optimal solution in the different COPs.

We observe that the success probability of the optimal solutions using LR-QAOA for the different COPs seems to scale as $probability(x^*) \approx 1/2^{(\eta N_q/p)}$ for a constant η . We add further evidence that this is the case using W-MaxCut, MaxCut, Max-2-SAT, and Max-3-SAT with up to 42 qubits. Using $p = N_q$, we find that the $probability(x^*) = cte$ remains nearly constant for W-MaxCut, MaxCut, and Max-3-SAT. The Max-2-SAT case is an exception, using $p = N_q$, it already shows an exponential decay in the probability of success. We think this is a consequence of problems with a

high concentration of solutions close to the optimal solution. With all of this information, we conjecture that $\text{probability}(x^*) = 1/2^{(\eta N_q/p)}$ for general problems.

This conjecture can be taken as an estimate of the expected performance of LR-QAOA. It implies that LR-QAOA can solve typical cases of NP-Hard problems in polynomial time. However, we also find particular cases where LR-QAOA does not follow a $\text{probability}(x^*) = \text{cte}$ when $p = N_q$. In such cases, there is a sub-exponential speedup. It is still possible that in the general case a $p = \text{Poly}(N_q)$ holds the $\text{probability}(x^*) = \text{cte}$. However, we suspect that in the limit, i.e., a random oracle with just one optimal solution and the first excited state completely degenerated, a performance similar to that of Grover's algorithm will be obtained. We also observed that the approximation ratio increases with p and seems constant at a specific p independently of the problem size for MaxCut, W-MaxCut, and 3-MaxCut problems.

We compare SA, LR-QAOA, and CPL EX in terms of TTS for fully connected W-MaxCut problems. In the largest case, $N_q = 42$, LR-QAOA has an improvement of 2 orders of magnitude compared to the other two solvers. We think there is a fundamental improvement in LR-QAOA. While any other classical solver needs time to learn the energy structure of the problem, LR-QAOA exploits the U_C phenomenon, Eq. 7, having the full energy information stored in the rotation of the amplitudes. This information is then efficiently used by the U_B gate to amplify the probability of obtaining low-energy solutions.

Moreover, we find that LR-QAOA is resilient to noise. This is important as we are at a stage where quantum computers have moderate noise. We simulate a MIS using LR-QAOA with $p = 80$ and at $p = 15$ we add a layer of X gates to see how the algorithm evolves under this noise. We find that there is an interplay between noise and the algorithm trying to get to the ground state. If the noise is low enough, the own algorithm corrects it to some extent. We use depolarizing noise for the simulation of a 10-qubit W-MaxCut problem using the LR-QAOA protocol and find that it fits well with the experimental results on *ionq-aria*.

We find that there is an effective number of layers for what the real device shows the best performance. We call it the p_{eff} , this parameter can be used to measure the progress of quantum technology for combinatorial optimization. For IBM Eagle devices and *ionq-aria* $p_{\text{eff}} = 10$ and for *quantinuum.H2* is $p_{\text{eff}} = 50$ for a 1D topology problem. We expect the p_{eff} decreases for a fully connected graph problem.

The experimental results make us optimistic that in the near future, we will start to compete against classical solvers to find the best-known solutions for COPs. For example, *quantinuum.H2* already shows its peak performance at $p = 50$ and loses little performance at $p = 100$. At the peak point, the device reaches the best approximation ratio of $r = 0.95$ and $\text{probability}(x^*) = 0.08$ for a 25-qubit problem. On the other hand, the inaccuracy of *ibm-brisbane* is still compensated by its sample rate for the same problem. The next step, left for future work, is to test fully connected W-MaxCut problems where *quantinuum.H2* and *ionq-aria* have a clear advantage because they have a fully connected layout.

The 109-qubit experiment already in the regime of quantum supremacy constitutes indirect proof that the LR-QAOA protocol works for larger cases. These cases constitute a set of experiments that cannot be simulated exactly on classical computers, and even approximations will result hard as p grows. We find that some information on the LR-QAOA algorithm remains for the largest case, $N_q = 109$ and $p = 100$.

DATA AVAILABILITY

The datasets for W-MaxCut problems used and/or analyzed during the current study are available from the following publicly accessible repository <https://jugit.fz-juelich.de/qip/lr-qaoa>. The other datasets are available from the corresponding author upon reasonable request.

ACKNOWLEDGMENTS

The authors thank Dennis Willsch, Vrinda Mehta, Hans De Raedt, and Fengping Jin for the insightful discussions and suggestions made for the present work. J. A. Montanez-Barrera acknowledges support from the German Federal Ministry of Education and Research (BMBF), funding program Quantum technologies - from basic research to market, project QSolid (Grant No. 13N16149). The authors gratefully acknowledge the Gauss Centre for Supercomputing e.V. (www.gauss-centre.eu) for funding this project by providing computing time on the GCS Supercomputer JUWELS at Jülich Supercomputing Centre (JSC).

This research used resources of the Oak Ridge Leadership Computing Facility for the experiments on *quantinuum.H2*, which is a DOE Office of Science User Facility supported under Contract DE-AC05-00OR22725.

-
- [1] E. Farhi, J. Goldstone, and S. Gutmann, (2014).
 - [2] A. Lucas, *Frontiers in Physics* **2**, 1 (2014), arXiv:1302.5843.

- [3] G. Kochenberger, J. K. Hao, F. Glover, M. Lewis, Z. Lü, H. Wang, and Y. Wang, *Journal of Combinatorial Optimization* **28**, 58 (2014).

- [4] E. Farhi, J. Goldstone, S. Gutmann, and M. Sipser, (2000), arXiv:0001106 [quant-ph].
- [5] M. P. Harrigan, K. J. Sung, M. Neeley, K. J. Satzinger, F. Arute, K. Arya, J. Atalaya, J. C. Bardin, R. Barends, S. Boixo, M. Broughton, B. B. Buckley, D. A. Buell, B. Burkett, N. Bushnell, Y. Chen, Z. Chen, Ben Chiaro, R. Collins, W. Courtney, S. Demura, A. Dunsworth, D. Eppens, A. Fowler, B. Foxen, C. Gidney, M. Giustina, R. Graff, S. Habegger, A. Ho, S. Hong, T. Huang, L. B. Ioffe, S. V. Isakov, E. Jeffrey, Z. Jiang, C. Jones, D. Kafri, K. Kechedzhi, J. Kelly, S. Kim, P. V. Klimov, A. N. Korotkov, F. Kostritsa, D. Landhuis, P. Laptev, M. Lindmark, M. Leib, O. Martin, J. M. Martinis, J. R. McClean, M. McEwen, A. Megrant, X. Mi, M. Mohseni, W. Mruczkiewicz, J. Mutus, O. Naaman, C. Neill, F. Neukart, M. Y. Niu, T. E. O’Brien, B. O’Gorman, E. Ostby, A. Petukhov, H. Putterman, C. Quintana, P. Roushan, N. C. Rubin, D. Sank, A. Skolik, V. Smelyanskiy, D. Strain, M. Streif, M. Szalay, A. Vainsencher, T. White, Z. J. Yao, P. Yeh, A. Zalcman, L. Zhou, H. Neven, D. Bacon, E. Lucero, E. Farhi, and R. Babbush, *Nature Physics* **17**, 332 (2021), 2004.04197.
- [6] P. Niroula, R. Shaydulin, R. Yalovetzky, P. Minssen, D. Herman, S. Hu, and M. Pistoia, (2022), arXiv:2206.06290.
- [7] R. Shaydulin, P. C. Lotshaw, J. Larson, J. Ostrowski, and T. S. Humble, *ACM Transactions on Quantum Computing* **4**, 1 (2023), arXiv:2201.11785.
- [8] M. Ohzeki, *Scientific Reports* **10**, 1 (2020), arXiv:2002.05298.
- [9] M. Cerezo, A. Arrasmith, R. Babbush, S. C. Benjamin, S. Endo, K. Fujii, J. R. McClean, K. Mitarai, X. Yuan, L. Cincio, and P. J. Coles, *Nature Reviews Physics* **3**, 625 (2021), arXiv:2012.09265.
- [10] L. Bittel and M. Kliesch, *Physical Review Letters* **127**, 120502 (2021), arXiv:2101.07267.
- [11] V. Kremenetski, T. Hogg, S. Hadfield, S. J. Cotton, and N. M. Tubman, (2021), arXiv:2108.13056.
- [12] G. Koßmann, L. Binkowski, L. van Luijk, T. Ziegler, and R. Schwonnek, , 1 (2022), arXiv:2210.12406.
- [13] L. Zhou, S. T. Wang, S. Choi, H. Pichler, and M. D. Lukin, *Physical Review X* **10**, 1 (2020), arXiv:1812.01041.
- [14] B. Apolloni, C. Carvalho, and D. de Falco, *Stochastic Processes and their Applications* **33**, 233 (1989).
- [15] D. De Falco and D. Tamascelli, *RAIRO - Theoretical Informatics and Applications* **45**, 99 (2011), arXiv:1107.0794.
- [16] F. G. S. L. Brandao, M. Broughton, E. Farhi, S. Gutmann, and H. Neven, , 1 (2018), arXiv:1812.04170.
- [17] D. Willsch, M. Willsch, F. Jin, K. Michielsen, and H. De Raedt, *Computer Physics Communications* **278**, 108411 (2022), arXiv:2104.03293.
- [18] J. A. Montanez-Barrera, D. Willsch, and K. Michielsen, , 1 (2024), arXiv:2402.05549.
- [19] V. Kremenetski, A. Apte, T. Hogg, S. Hadfield, and N. M. Tubman, , 1 (2023), arXiv:2305.04455.
- [20] D. Krause, *Journal of large-scale research facilities JL-SRF* **5**, A135 (2019).
- [21] D. Alvarez, *J. of Large-Scale Res. Facil.* **7**, A183 (2021).
- [22] G. Gutin and A. Yeo, **1**, 1 (2021), arXiv:2104.05536.
- [23] C. Paradimitriou and M. Yannakakis, *Journal of computer and system sciences* **43**, 425 (1991).
- [24] S. A. Moses, C. H. Baldwin, M. S. Allman, R. Ancona, L. Ascarrunz, C. Barnes, J. Bartolotta, B. Bjork, P. Blanchard, M. Bohn, J. G. Bohnet, N. C. Brown, N. Q. Burdick, W. C. Burton, S. L. Campbell, J. P. Campora, C. Carron, J. Chambers, J. W. Chan, Y. H. Chen, A. Chernoguzov, E. Chertkov, J. Colina, J. P. Curtis, R. Daniel, M. Decross, D. Deen, C. Delaney, J. M. Dreiling, C. T. Ertsgaard, J. Esposito, B. Estey, M. Fabrikant, C. Figgatt, C. Foltz, M. Foss-Feig, D. Francois, J. P. Gaebler, T. M. Gatterman, C. N. Gilbreth, J. Giles, E. Glynn, A. Hall, A. M. Hankin, A. Hansen, D. Hayes, B. Higashi, I. M. Hoffman, B. Horning, J. J. Hout, R. Jacobs, J. Johansen, L. Jones, J. Karcz, T. Klein, P. Lauria, P. Lee, D. Liefer, S. T. Lu, D. Lucchetti, C. Lytle, A. Malm, M. Matheny, B. Mathewson, K. Mayer, D. B. Miller, M. Mills, B. Neyenhuis, L. Nugent, S. Olson, J. Parks, G. N. Price, Z. Price, M. Pugh, A. Ransford, A. P. Reed, C. Roman, M. Rowe, C. Ryan-Anderson, S. Sanders, J. Sedlacek, P. Shevchuk, P. Siegfried, T. Skripka, B. Spaun, R. T. Sprenkle, R. P. Stutz, M. Swallows, R. I. Tobey, A. Tran, T. Tran, E. Vogt, C. Volin, J. Walker, A. M. Zolot, and J. M. Pino, *Physical Review X* **13**, 41052 (2023), 2305.03828.
- [25] IBM Q team, “Qiskit: An open-source framework for quantum computing,” (2021), <https://doi.org/10.5281/zenodo.2573505>, release 0.39.4.
- [26] A. Montanez-Barrera, D. Willsch, A. Maldonado-Romo, and K. Michielsen, *Quantum Science and Technology* , 23 (2024), arXiv:2211.13914.
- [27] S. Hadfield, T. Hogg, and E. G. Rieffel, *Quantum Science and Technology* **8**, 1 (2023), arXiv:2105.06996.
- [28] J. A. Montanez-Barrera, P. van den Heuvel, D. Willsch, and K. Michielsen, 2023 IEEE International Conference on Quantum Computing and Engineering (QCE) **01**, 535 (2023), arXiv:2305.18757.
- [29] A. Wald and J. Wolfowitz, *The Annals of Mathematical Statistics* **15**, 358 (1944).
- [30] S. Kirkpatrick, C. D. Gelatt, and M. P. Vecchi, *Science* **220**, 671 (1983).
- [31] C. Blik, P. Bonami, and A. Lodi (2014).
- [32] “IonQ Aria Quantum System,” <https://ionq.com/quantum-systems/aria>.
- [33] IBM Quantum Blog, “Eagle Quantum Processor,” (2022).
- [34] D. C. McKay, I. Hincks, E. J. Pritchett, M. Carroll, L. C. G. Govia, and S. T. Merkel, (2023), arXiv:2311.05933.
- [35] V. R. Pascuzzi, A. He, C. W. Bauer, W. A. de Jong, and B. Nachman, *Phys. Rev. A* **105**, 042406 (2022).
- [36] L. K. Grover, *Proceedings of the Annual ACM Symposium on Theory of Computing Part F129452*, 212 (1996), arXiv:9605043 [quant-ph].
- [37] J. Wurtz and D. Lykov, (2021), arXiv:2107.00677.
- [38] J. Hastad, *Conference Proceedings of the Annual ACM Symposium on Theory of Computing* , 1 (1997).
- [39] D. P. Williamson and M. Goemans, *Science* **42**, 1115 (1994).
- [40] S. Khot, in *Proceedings of the Thirty-Fourth Annual ACM Symposium on Theory of Computing*, STOC ’02 (Association for Computing Machinery, New York, NY, USA, 2002) p. 767–775.
- [41] S. Khot, G. Kindler, E. Mossel, and R. O’Donnell, *SIAM Journal on Computing* **37**, 319 (2007).

- [42] P. Cheeseman, B. Kanefsky, and W. M. Taylor, The 12nd International Joint Conference on Artificial Intelligence , 331 (1991).
- [43] S. Zielinski, J. Nüßlein, J. Stein, T. Gabor, C. Linnhoff-Popien, and S. Feld, *Electronics (Switzerland)* **12** (2023), 10.3390/electronics12163492, arXiv:2305.02659.
- [44] V. Mehta, F. Jin, H. De Raedt, and K. Michielsen, *Physical Review A* **104**, 1 (2021), arXiv:arXiv:2106.04864v2.
- [45] C. H. Bennett, E. Bernstein, G. Brassard, and U. Vazirani, *SIAM Journal on Computing* **26**, 1510 (1997), arXiv:9701001 [quant-ph].
- [46] F. Arute, K. Arya, R. Babbush, D. Bacon, J. C. Bardin, R. Barends, R. Biswas, S. Boixo, F. G. Brandao, D. A. Buell, B. Burkett, Y. Chen, Z. Chen, B. Chiaro, R. Collins, W. Courtney, A. Dunsworth, E. Farhi, B. Foxen, A. Fowler, C. Gidney, M. Giustina, R. Graff, K. Guerin, S. Habegger, M. P. Harrigan, M. J. Hartmann, A. Ho, M. Hoffmann, T. Huang, T. S. Humble, S. V. Isakov, E. Jeffrey, Z. Jiang, D. Kafri, K. Kechedzhi, J. Kelly, P. V. Klimov, S. Knysh, A. Korotkov, F. Kostritsa, D. Landhuis, M. Lindmark, E. Lucero, D. Lyakh, S. Mandrà, J. R. McClean, M. McEwen, A. Megrant, X. Mi, K. Michielsen, M. Mohseni, J. Mutus, O. Naaman, M. Neeley, C. Neill, M. Y. Niu, E. Ostby, A. Petukhov, J. C. Platt, C. Quintana, E. G. Rieffel, P. Roushan, N. C. Rubin, D. Sank, K. J. Satzinger, V. Smelyanskiy, K. J. Sung, M. D. Trevithick, A. Vainsencher, B. Villalonga, T. White, Z. J. Yao, P. Yeh, A. Zalcman, H. Neven, and J. M. Martinis, *Nature* **574**, 505 (2019).
- [47] Y. Kim, A. Eddins, S. Anand, K. X. Wei, E. van den Berg, S. Rosenblatt, H. Nayfeh, Y. Wu, M. Zaletel, K. Temme, and A. Kandala, *Nature* **618**, 500 (2023).
- [48] E. Pednault, J. A. Gunnels, G. Nannicini, L. Horesh, T. Magerlein, E. Solomonik, E. W. Draeger, E. T. Holland, and R. Wisnieff, , 1 (2017), arXiv:1710.05867.
- [49] T. Begušić, J. Gray, and G. K. L. Chan, *Science Advances* **10**, 1 (2024), arXiv:2308.05077.
- [50] M. S. Jattana, F. Jin, H. De Raedt, and K. Michielsen, *Physical Review Applied* **19**, 1 (2023), arXiv:2202.10130.

Appendix A: Supplementary Material

1. Max-3-SAT problem

The 3-SAT problem belongs to the family of Boolean satisfiability problems (SAT). 3-SAT has a specific structure called conjunctive normal form (CNF) which is described by

$$\varphi = \bigwedge_i \left(\bigvee_j l_{ij} \right) \quad (\text{A1})$$

where l_{ij} are literals, i.e., any elements for the set of variables $x_k \forall k \in \{0, \dots, N_V - 1\}$ or its negation $\neg x_k$, for N_V variables. The \vee and \wedge represent the Boolean operations OR and AND, respectively. The terms $(\bigvee_j l_{ij})$ are called clauses and in the case of 3-SAT, there are 3 literals for each clause. The total number of clauses is N_C .

Constructing the QUBO formulation for a individual clause, $C_i = (x_0 \vee x_1 \vee x_2)$ is given by

$$(x_0 \vee x_1 \vee x_2) = -(x_0 + x_1 + x_2 - x_0x_1 - x_0x_2 - x_1x_2 + x_0x_1x_2), \quad (\text{A2})$$

and the Hamiltonian representation of this QUBO in terms of the spin variables $x_i = (1 + s_i)/2$ is given by

$$(x_0 \vee x_1 \vee x_2) = -\frac{1}{8} (s_0 + s_1 + s_2 - s_0s_1 - s_0s_2 - s_1s_2 + s_0s_1s_2 + 7), \quad (\text{A3})$$

The three body interactions, $s_0s_1s_2$, in Eq. A3, can be represented by the circuit shown in Fig. 10 of [50]. It allows to use $N_q = N_V$ qubits to describe the problem contrary to other QUBO formulations where it is needed $N_q = N_V + N_C$ variables [43]. The Max-3-SAT version of the problem consists of finding the solution that maximizes the number of clauses satisfied.